

# Many-body theory for positronium-atom interactions

D. G. Green,<sup>\*</sup> A. R. Swann,<sup>†</sup> and G. F. Gribakin<sup>‡</sup>

Centre for Theoretical Atomic, Molecular, and Optical Physics, School of Mathematics and Physics,  
Queen's University Belfast, Belfast BT7 1NN, Northern Ireland, United Kingdom

(Dated: December 14, 2024)

A many-body-theory approach has been developed to study positronium-atom interactions. As first applications, we calculate the elastic scattering and momentum-transfer cross sections and the pickoff annihilation rate  ${}^1Z_{\text{eff}}$  for Ps collisions with He and Ne. The cross section for He is in agreement with previous coupled-state calculations, and the momentum-transfer cross section for Ne agrees with available experimental data.  ${}^1Z_{\text{eff}}$  is found to be 0.13 and 0.26 for He and Ne, respectively, in excellent agreement with the measured values.

Positronium (Ps) is a light and simple “atom” consisting of an electron and its antiparticle, the positron. It is important for precision tests of QED [1] and for understanding galactic positron annihilation [2], and has numerous applications, from probing free space in condensed matter systems [3] to making antihydrogen [4] and studying free fall of antimatter [5]. These applications require understanding of Ps interaction with normal matter, which is far from complete. Thus, recent experiments on Ps scattering on noble-gas atoms revealed some unexpected trends, e.g., that the scattering cross section becomes very small at low Ps energies [6]. Overall, there is a large uncertainty in the existing Ps-atom scattering data [7], while calculations of the rate of *pickoff* annihilation on noble gases (where the positron from Ps annihilates with an atomic electron) [8–14] underestimate the experimental data [15, 16] by as much as a factor of ten.

The theoretical description of Ps-atom interactions is challenging because of the composite nature of both the target and projectile and a significant cancellation between the repulsive static Ps-atom interaction and van-der-Waals-type attraction. Accurate calculations must account for dynamical distortion of both objects during the collision, which has only been achieved for simple targets, i.e., hydrogen and helium [17]. Calculations of pickoff annihilation require account of important short-range electron-positron correlations; these are described via corrections to the annihilation vertex [18–21] and have been neglected in all previous calculations.

Many-body theory (MBT) provides a powerful, natural, and systematic method of accounting for the distortion of both objects and the electron-positron correlation effects. It provided an accurate description of low-energy electron-atom scattering [22–27] and positron interaction with atoms [19, 20, 28–32], with scattering cross sections, annihilation rates, and  $\gamma$  spectra all found to be in excellent agreement with experiment.

In this Letter we show how to describe Ps interaction with a many-electron atom by combining the MBT description of electron-atom and positron-atom interactions, and including the important effect of screening of the electron-positron Coulomb interaction by the atom. As first applications of the theory, we calculate phase shifts, elastic-scattering and momentum-transfer cross sections, and the pickoff annihilation rate  ${}^1Z_{\text{eff}}$  for Ps on He and Ne. The cross sections are found to be in agreement with previous coupled-state [17] and model van der Waals [7] calculations. By accounting for

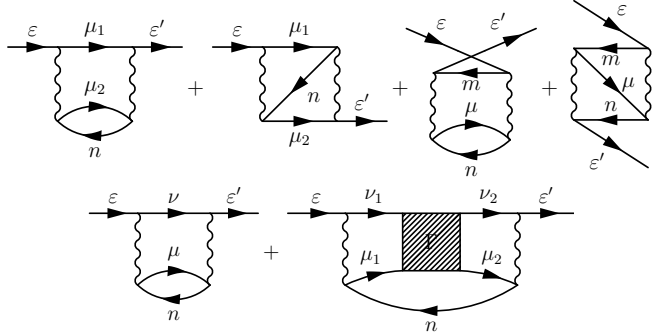


FIG. 1. The main contributions to the self-energy of the electron (top line) and positron (bottom line) in the field of the atom. Lines labeled  $\varepsilon$  represent the electron or positron HF wave function. Lines labeled  $\nu$  ( $\mu$ ) represent positron (excited electron) states, which are summed over. Lines labeled  $n$  and  $m$  represent holes in the atomic ground state. Wavy lines represent Coulomb interactions. The shaded  $\Gamma$  block represents the sum of the electron-positron ladder-diagram series [19, 30], which accounts for virtual Ps formation.

electron-positron correlation corrections to the annihilation vertex, we obtain values of  ${}^1Z_{\text{eff}}$  in excellent agreement with experiment [15]. Atomic units (a.u.) are used throughout.

*MBT of electron- and positron-atom interactions.*—MBT describes an electron or positron in the field of a many-electron atom via the Dyson equation for the (quasiparticle) wave function  $\psi_{\varepsilon}$  [33]:

$$(\hat{H}_0^{\pm} + \hat{\Sigma}_{\varepsilon}^{\pm})\psi_{\varepsilon}^{\pm}(\mathbf{r}) = \varepsilon\psi_{\varepsilon}^{\pm}(\mathbf{r}). \quad (1)$$

Here  $\hat{H}_0^{\pm}$  is the zeroth-order Hamiltonian, e.g., that of the electron (–) or positron (+) in the field of the Hartree-Fock (HF) ground-state atom, and  $\hat{\Sigma}_{\varepsilon}^{\pm}$  is the nonlocal, energy-dependent correlation potential [34], given by the irreducible self-energy of the electron or positron in the field of the atom. Equation (1) can be solved separately for each partial wave, with the wave function of central-field form  $\psi_{\varepsilon}^{\pm}(\mathbf{r}) = r^{-1}\tilde{P}_{\varepsilon\ell}^{\pm}(r)Y_{\ell m}(\hat{\mathbf{r}})$ , where  $Y_{\ell m}$  is a spherical harmonic with angular momentum  $\ell$  and projection  $m$ . Rather than computing the self-energy  $\Sigma_E^{\pm}(\mathbf{r}, \mathbf{r}')$  in the coordinate basis, it is more convenient to work with its matrix elements  $\langle \varepsilon' | \Sigma_E^{\pm} | \varepsilon \rangle$  in the HF basis  $\{\varphi_{\varepsilon}^{\pm}\}$ , where  $H_0^{\pm}\varphi_{\varepsilon}^{\pm} = \varepsilon\varphi_{\varepsilon}^{\pm}$ ,  $\varphi_{\varepsilon}^{\pm}(\mathbf{r}) = r^{-1}P_{\varepsilon\ell}^{\pm}(r)Y_{\ell m}(\hat{\mathbf{r}})$ , and  $\langle \varepsilon' | \Sigma_E^{\pm} | \varepsilon \rangle = \int P_{\varepsilon'\ell}^{\pm}(r')\Sigma_{E\ell}^{\pm}(r, r')P_{\varepsilon\ell}^{\pm}(r)dr dr'$ , with  $\Sigma_{E\ell}^{\pm}$  the self-energy for partial wave  $\ell$ . Using the completeness of the

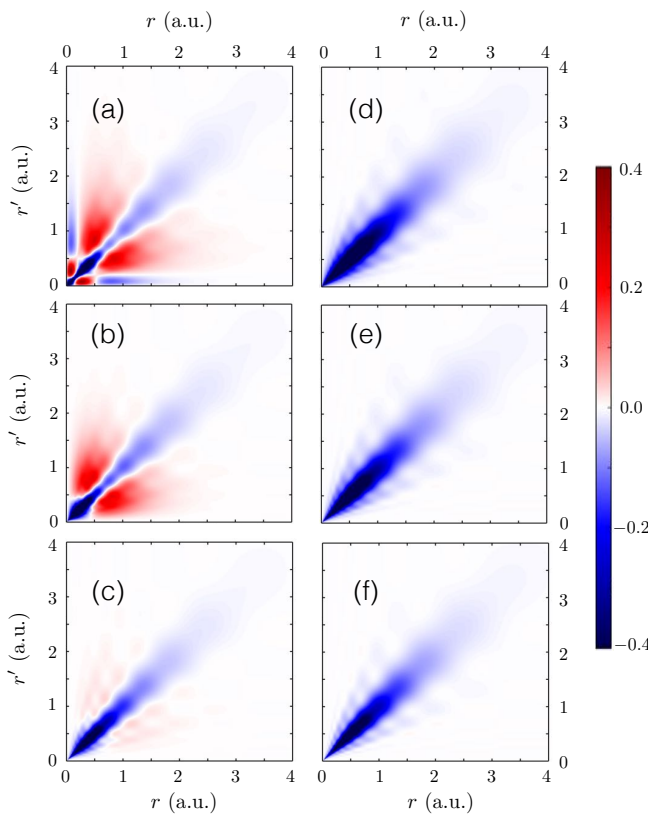


FIG. 2. Self-energy  $\Sigma_{E\ell}^\pm(r, r')$  at  $E = 0$  for electron (a)–(c) and positron (d)–(f) in the field of Ne, for  $\ell = 0, 1$ , and  $2$ , respectively.

basis, it can be expressed as

$$\Sigma_{E\ell}^\pm(r, r') = \sum_{\varepsilon, \varepsilon'} P_{\varepsilon' \ell}^\pm(r') \langle \varepsilon' | \Sigma_{E\ell}^\pm | \varepsilon \rangle P_{\varepsilon \ell}^\pm(r). \quad (2)$$

Figure 1 shows the main contributions to the matrix elements of  $\Sigma_E^-$  (top) and  $\Sigma_E^+$  (bottom). For the electron, the first diagram accounts for the attractive long-range polarization potential  $-\alpha_d/2r^4$ , where  $\alpha_d$  is the dipole polarizability of the atom. The other three diagrams contribute only at short range. Including these second-order diagrams in  $\Sigma_E^-$  gives a good description of the electron–noble-gas-atom system [23–26][35]. For the positron, the first diagram gives rise to a similar long-range polarization potential as for the electron. In addition, there is an important contribution of virtual Ps formation [19, 29, 30]. It is described by the second diagram in which the  $\Gamma$  block represents the sum of the infinite electron-positron ladder-diagram series [30]. We calculate the self-energy as described in Ref. [19], using a  $B$ -spline basis with 40 splines of order 6 defined over an exponential knot sequence, discretizing the continuum by confining the system in a spherical cavity of radius 30 a.u. The corresponding electron and positron basis sets provide an efficient spanning of the continuum and rapid convergence of the sums over intermediate states.

The correlation potential described by the self-energy is essentially nonlocal. It is also quite different for the electron

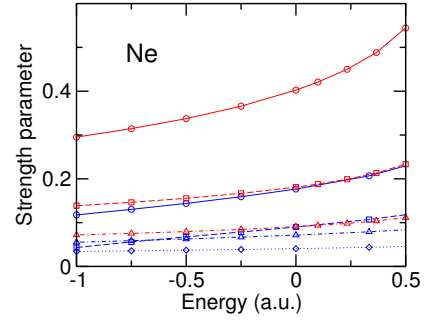


FIG. 3. The dimensionless strength parameter  $S_{E\ell}^\pm$  of the correlation potentials for the electron (blue) and positron (red) in the field of Ne, as a function of energy  $E$ , for  $\ell = 0$  (circles),  $\ell = 1$  (squares),  $\ell = 2$  (triangles), and  $\ell = 3$  (diamonds). Lines are interpolants.

and positron, and for different electron and positron partial waves. Figure 2 shows  $\Sigma_{E\ell}^\pm(r, r')$  for the  $s$ ,  $p$ , and  $d$  waves in Ne, calculated at  $E = 0$ . The main feature is a “valley” along the diagonal  $r = r'$ , whose width characterizes the degree to which  $\hat{\Sigma}^\pm$  is nonlocal. The main contribution to electron- and positron-atom attraction comes from  $r \gtrsim 1$  a.u. (i.e., outside the atom). Here,  $\Sigma_{E\ell}^+(r, r')$  is more negative than  $\Sigma_{E\ell}^-(r, r')$ , meaning stronger attraction for the positron. As a consequence of the Pauli principle, the correlation potential for the electron is quite different for different partial waves. It is also significantly more nonlocal than that of the positron, with prominent repulsive contributions for the  $s$  and  $p$  waves. These features are due to the contribution of the second, exchange diagram to  $\Sigma_{E\ell}^-(r, r')$ . For both the electron and positron,  $\Sigma_{E\ell}^\pm$  becomes increasingly local for larger  $\ell$ .

The electron and positron correlation potentials are also energy dependent. This dependence can be analyzed using the dimensionless strength parameter  $S_{E\ell}^\pm = -\sum_{\varepsilon > 0} \langle \varepsilon | \Sigma_{E\ell}^\pm | \varepsilon \rangle / \varepsilon$  [36]. Figure 3 shows  $S_{E\ell}^\pm$  for Ne, as a function of energy for electron and positron  $s$ ,  $p$ ,  $d$ , and (for the electron)  $f$  waves. It confirms that the correlation potential is stronger for the positron. It also shows that its energy dependence is relatively weak on the energy scale of Ps (0.25 a.u.). This is important for the description of Ps-atom interaction, as it allows us to use  $\Sigma_{E\ell}^\pm(r, r')$  calculated for a fixed energy ( $E = 0$ ).

*MBT of Ps-atom interactions.*— The wave function  $\Psi$  of Ps in the field of the atom satisfies the two-particle Dyson equation

$$(\hat{H}_0^- + \hat{\Sigma}_{\varepsilon^-}^- + \hat{H}_0^+ + \hat{\Sigma}_{\varepsilon^+}^+ + V + \delta V_E) \Psi = E \Psi, \quad (3)$$

where  $V$  is the electron-positron Coulomb interaction and  $\delta V_E$  is the screening correction due to polarization of the atom [37]. The diagrams for  $\delta V_E$  are shown in Fig. 4. Diagram (b) describes screening of  $V$  by the atomic electrons. They are essential for canceling the long-range  $r^{-4}$  polarization attraction and making the long-range Ps-atom interaction of the required  $R^{-6}$  van der Waals form, where  $R$  is the distance between the Ps center of mass and the atom. The exchange corrections (c) and (d) are typically much smaller. They also partly cancel each other due to their opposite signs, and can be neglected.

The Ps eigenstates with angular momentum  $J$  and parity  $\Pi$ , are constructed from the single-particle Dyson states [7, 38]

$$\Psi_{J\Pi}(\mathbf{r}_e, \mathbf{r}_p) = \sum_{\mu, \nu} C_{\mu\nu}^{J\Pi} \psi_{\mu}^{-}(\mathbf{r}_e) \psi_{\nu}^{+}(\mathbf{r}_p), \quad (4)$$

with coefficients  $C_{\mu\nu}^{J\Pi}$ . Solution of Eq. (3) reduces to the matrix eigenvalue problem  $\mathbf{HC} = E\mathbf{C}$  for the Hamiltonian matrix

$$\langle \nu' \mu' | H | \mu \nu \rangle = (\varepsilon_{\mu} + \varepsilon_{\nu}) \delta_{\mu' \mu} \delta_{\nu' \nu} + \langle \nu' \mu' | V + \delta V_E | \mu \nu \rangle, \quad (5)$$

where  $\mathbf{C}$  is the vector of coefficients. We consider  $J^{\Pi} = 0^+$ ,  $1^-$ , and  $2^+$  to investigate Ps  $S$ -,  $P$ -, and  $D$ -wave scattering, respectively. To ensure accurate description of Ps states by Eq. (4), we confine the electron and positron states to a cavity of radius  $R_c = 10\text{--}16$  a.u. [38]. To accurately represent the positive-energy ‘‘continuum’’ in the cavity, we use a second  $B$ -spline basis of 60 splines of order 9 defined over a quadratic-linear knot sequence [7]. Given the decrease of  $\Sigma_{E\ell}^{\pm}$  with the single-particle angular momenta  $\ell$  (see Figs. 2 and 3), we find that it is sufficient to use Dyson states in Eq. (4) for  $\ell \leq 3$  and use HF states for higher  $\ell$ . We exploit the weak energy dependence of  $\Sigma_E^{\pm}$  and  $\delta V_E$  by evaluating them at  $E = 0$ . Calculations are performed with different numbers of radial states and angular momenta included in Eq. (4), up to  $n_{\max} = 20$  and  $\ell_{\max} = 20$ . Accurate Ps states are found by extrapolating to  $n_{\max} \rightarrow \infty$  and  $\ell_{\max} \rightarrow \infty$  (see Ref. [38] for details).

*Ps scattering on He and Ne.*—As a first application, we calculate the phase shifts and cross sections for Ps scattering on He and Ne. The phase shifts are determined from the Ps energy eigenvalues using the boundary condition on the Ps center-of-mass motion at the cavity wall, as described in Ref. [7]. Calculations were performed using cavity radii of 10, 12, 14, and 16 a.u. Effective-range-type fits were used to interpolate the  $S$ ,  $P$ , and  $D$  phase shifts calculated at the discrete values of the Ps center-of-mass momentum  $K$ . These fits were used to determine the scattering length and the partial contributions to the elastic and momentum-transfer cross sections.

The partial and total elastic scattering cross sections are shown in Fig. 5 (a) and (b) for He and Ne, respectively. Comparing with the frozen-target (FT) results [obtained by neglecting  $\hat{\Sigma}_{\varepsilon}^{\pm}$  and  $\delta V_E$  in Eq. (3)], we see that correlations partially cancel the FT Ps-atom repulsion and reduce the cross sections. For He, the  $S$ -wave contribution dominates across the range of

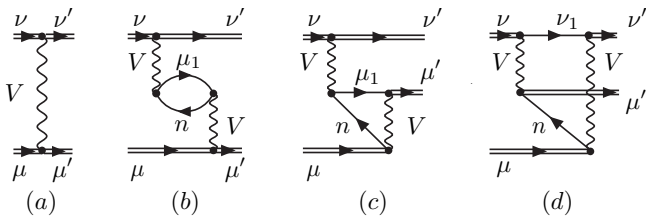


FIG. 4. The main contributions to the electron-positron interaction in Ps: (a) the bare Coulomb interaction  $V$ ; (b)–(d), screening  $\delta V_E$  with exchange contributions (with mirror images). Double lines labeled  $\nu$  ( $\mu$ ) represent positron (electron) Dyson states in the field of the atom.

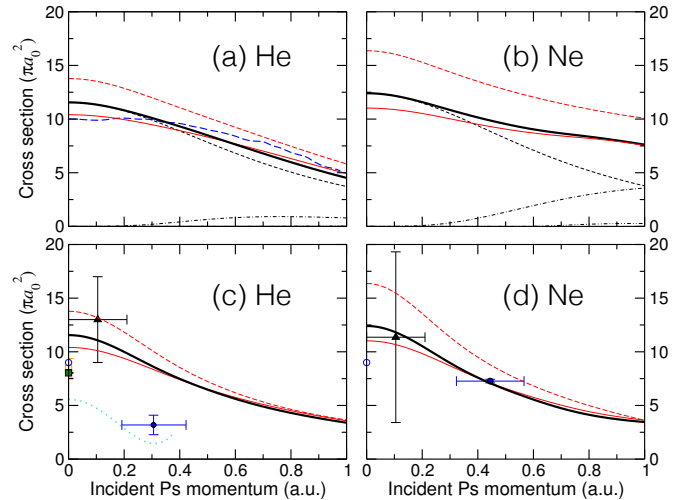


FIG. 5. Elastic-scattering cross sections for Ps on He (a) and Ne (b): total cross section calculated using MBT (thick solid line), with  $S$ - (dashed black line),  $P$ - (dot-dashed black line), and  $D$ -wave (dot-dot-dashed black line) partial contributions; FT (dashed red line) and FT+vdW (thin solid red line) calculations of Ref. [7]. Also shown for He is the 9-Ps-9-He-state calculation of Walters *et al.* [17] (thick dashed blue line). Momentum-transfer cross sections for Ps on He (c) and Ne (d) use the same symbols as in (a) and (b). Also shown are the experimental results [39] (open square), [40] (filled square), [41] (open circle), [42] (filled circle), [43] (triangle), and [44] (dotted turquoise line).

momenta considered, but for Ne, the  $P$ -wave contribution becomes comparable at  $K \approx 1$  a.u. For He, the total elastic cross section is in good agreement with the 9-Ps-9-He coupled-state calculation of Walters *et al.* [17] and is close to the calculation in which a model van-der-Waals potential was added to the FT Ps-atom interaction (FT+vdW) [7] for  $K \gtrsim 0.5$  a.u. [45]. The MBT scattering length of 1.70 a.u. compares well with the value of 1.6 a.u. obtained in Ref. [17]. It is  $\sim 10\%$  smaller than the FT value (1.86 a.u. [7]), highlighting the importance of including distortion of the target. For Ne, the MBT scattering length of 1.76 a.u. is  $\sim 15\%$  smaller than the FT value (2.02 a.u.) but close to the FT+vdW result (1.66 a.u. [7]). The relatively small effect of the correlations, seen as the difference between the MBT and FT calculations, is due to cancellation of the positron- and electron-atom attraction ( $\hat{\Sigma}_{\varepsilon}^{\pm}$ ) and the effect of screening  $\delta V_E$ .

Regarding the momentum-transfer cross sections [Fig. 5 (c) and (d)], the MBT calculation gives results that are similar to the FT+vdW calculation [7], especially for  $K \gtrsim 0.5$  a.u. For He, our calculation lies within the error bars of the experimental result of Nagashima *et al.* [43] but is  $\sim 30\text{--}45\%$  larger than that of Canter *et al.* [39], Rytola *et al.* [40], and Coleman *et al.* [41]. The measurements of Skalsey *et al.* [42] and Engbrecht *et al.* [44] give much lower values. For Ne, there is agreement with the results of Skalsey *et al.* [42] and Nagashima *et al.* [43] but a  $\sim 40\%$  discrepancy with that of Coleman *et al.* [41]. Given the theoretical predictions, the experimental data for Ne displays a greater degree of consistency

TABLE I. Pickoff annihilation rates  ${}^1Z_{\text{eff}}$  for He and Ne at  $K = 0$ : best previous theory [13]; using frozen-target Ps wave function from Ref. [7]; present theory, zeroth-order approximation (MBT); present theory with enhancement factors (MBT-EF); and experiment [15].

Atom	Ref. [13]	FT [7]	MBT	MBT-EF	Exp. [15]
He	0.0378	0.0273	0.0411	0.131	0.125
Ne	0.0922	0.0512	0.0932	0.255	0.235

than for He.

*Calculation of pickoff annihilation rates  ${}^1Z_{\text{eff}}$ .*—The Ps pickoff annihilation rate in a gas is parametrized as  $\lambda = 4\pi r_0^2 c n_g {}^1Z_{\text{eff}}$ , where  $r_0$  is the classical electron radius,  $c$  is the speed of light,  $n_g$  is the number density of the gas, and  ${}^1Z_{\text{eff}}$  is the effective number of electrons per atom in a singlet state relative to the positron [8]. Our interest is in the value of  ${}^1Z_{\text{eff}}$  at small momenta, where only the  $S$ -wave contributes. In the zeroth-order, independent-particle approximation (IPA),

$${}^1Z_{\text{eff}} = \frac{1}{4} \sum_n \int |\Psi_{0^+}(\mathbf{r}_e, \mathbf{r}_p)|^2 |\varphi_n(\mathbf{r}_p)|^2 d\mathbf{r}_e d\mathbf{r}_p, \quad (6)$$

where the sum is over all HF orbitals  $\varphi_n$  occupied in the ground-state atom, and  $\Psi_{0^+}$  is normalized to a plane wave of the Ps center-of-mass motion far from the atom. Previous IPA calculations for He [7–13, 46] and Ne [7, 13] yielded values of  ${}^1Z_{\text{eff}}$  that underestimated experimental data by a factor of 3 or more (see Table I). These calculations neglected the short-range electron-positron correlations, which are known to enhance the annihilation rates by a factor 2–5 [20, 47].

We take account of the correlation corrections in  ${}^1Z_{\text{eff}}$  by augmenting Eq. (6) with electron-orbital- and positron-partial-wave-specific *enhancement factors* (EF), which were calculated in Refs. [20, 47]. Specifically, we perform calculations for the lowest-energy  $J^{\Pi} = 0^+$  eigenstate for  $R_c = 10, 12, 14$ , and 16 a.u., giving values of  ${}^1Z_{\text{eff}}$  for four different  $K$ . These values depend on the maximum numbers of partial waves  $\ell_{\text{max}}$  and radial states per partial wave  $n_{\text{max}}$  included in Eq. (4). We extrapolate in  $\ell_{\text{max}}$  as  ${}^1Z_{\text{eff}}(\ell_{\text{max}}, n_{\text{max}}) = {}^1Z_{\text{eff}}(\infty, n_{\text{max}}) + A(\ell_{\text{max}} + 1/2)^{-2}$  and subsequently in  $n_{\text{max}}$  as  ${}^1Z_{\text{eff}}(\infty, n_{\text{max}}) = {}^1Z_{\text{eff}} + \alpha n_{\text{max}}^{\beta}$ , where we typically find  $\beta \approx -4$  [48]. The Ps wave function is normalized to the center-of-mass plane wave by comparing the center-of-mass density away from the atom with  $\sin^2(KR + \delta_0)/K^2 R^2$  (see Ref. [49] for details). Finally, we fit the four values to the effective-range form  ${}^1Z_{\text{eff}}(K) \simeq {}^1Z_{\text{eff}}(0) + CK^2$  to deduce  ${}^1Z_{\text{eff}}(0)$ . The results are shown in Table I. Neglecting the enhancement factors, we find good agreement with the previous best zeroth-order results. Including the enhancement produces near-perfect agreement with experimental values for room-temperature Ps.

*Summary.*—The MBT of Ps interactions with atoms was presented and applied to calculate scattering cross sections and pickoff annihilation rates in He and Ne. The calculations show that the net effect of the dispersion interaction (electron and positron polarization of the atom and screening of the electron-positron Coulomb interaction by atomic electrons) is relatively

small, and close to that described by a model van der Waals potential with a short-range cutoff. The MBT gives pickoff annihilation rates in excellent agreement with experiment.

*Acknowledgments.*—DGG was supported by the EPSRC UK, grant EP/N007948/1. ARS was supported by the Department for Employment and Learning, Northern Ireland, UK, and is supported by the EPSRC UK, grant EP/R006431/1.

\* d.green@qub.ac.uk

† a.swann@qub.ac.uk

‡ g.gribakin@qub.ac.uk

- [1] S. G. Karshenboim, *Phys. Rep.* **422**, 1 (2005).
- [2] E. Churazov, S. Sazonov, S. Tsygankov, R. Sunyaev, and D. Varshalovich, *Mon. Not. R. Astron. Soc.* **411**, 1727 (2011).
- [3] D. W. Gidley, H. Peng, and R. S. Vallery, *Riv. Nuovo. Cimento* **36**, 49 (2006).
- [4] A. Kellerbauer, M. Amoretti, A. Belov, G. Bonomi, I. Boscolo, R. Brusa, M. Büchner, V. Byakov, L. Cabaret, C. Canali, C. Carrao, F. Castelli, S. Cialdi, M. de Combarieu, D. Comparat, G. Consolati, N. Djourelou, M. Doser, G. Drobyshev, A. Dupasquier, G. Ferrari, P. Forget, L. Formaro, A. Gervasini, M. Giannamarchi, S. Gnenenko, G. Gribakin, S. Hogan, M. Jacquay, V. Lagomarsino, G. Manuzio, S. Mariazzi, V. Matveev, J. Meier, F. Merkt, P. Nedelec, M. Oberthaler, P. Pari, M. Prevedelli, F. Quasso, A. Rotondi, D. Sillou, S. Stepanov, H. Stroke, G. Testera, G. Tino, G. Trénec, A. Vairo, J. Vigué, H. Walters, U. Warring, S. Zavatarelli, and D. Zvezhinskij, *Nucl. Instrum. Methods B* **266**, 351 (2008).
- [5] D. B. Cassidy, T. H. Hisakado, H. W. K. Tom, and A. P. Mills, Jr., *Phys. Rev. Lett.* **106**, 173401 (2011).
- [6] S. J. Brawley, S. E. Fayer, M. Shipman, and G. Laricchia, *Phys. Rev. Lett.* **115**, 223201 (2015).
- [7] A. R. Swann and G. F. Gribakin, *Phys. Rev. A* (2018), (accepted for publication), arXiv:1712.05127.
- [8] P. A. Fraser and M. Kraidy, *Proc. Phys. Soc.* **89**, 533 (1966).
- [9] P. A. Fraser, *J. Phys. B* **1**, 1006 (1968).
- [10] M. I. Barker and B. H. Bransden, *J. Phys. B* **1**, 1109 (1968).
- [11] R. J. Drachman and S. K. Houston, *J. Phys. B* **3**, 1657 (1970).
- [12] P. K. Biswas and S. K. Adhikari, *Chem. Phys. Lett.* **317**, 129 (2000).
- [13] J. Mitroy and I. A. Ivanov, *Phys. Rev. A* **65**, 012509 (2001).
- [14] J. Mitroy and M. W. J. Bromley, *Phys. Rev. A* **67**, 034502 (2003).
- [15] M. Charlton, *Rep. Prog. Phys.* **48**, 737 (1985).
- [16] H. Saito and T. Hyodo, *Phys. Rev. Lett.* **97**, 253402 (2006).
- [17] H. Walters, A. Yu, S. Sahoo, and S. Gilmore, *Nucl. Instrum. and Meth. B* **221**, 149 (2004).
- [18] L. J. M. Dunlop and G. F. Gribakin, *J. Phys. B* **39**, 1647 (2006).
- [19] D. G. Green, J. A. Ludlow, and G. F. Gribakin, *Phys. Rev. A* **90**, 032712 (2014).
- [20] D. G. Green and G. F. Gribakin, *Phys. Rev. Lett.* **114**, 093201 (2015).
- [21] D. G. Green and G. F. Gribakin, *Phys. Rev. A* **88**, 032708 (2013).
- [22] H. P. Kelly, *Phys. Rev.* **160**, 44 (1967).
- [23] M. Amusia, N. Cherepkov, L. Chernysheva, and S. Shapiro, *Phys. Lett. A* **46**, 387 (1974).
- [24] M. Y. Amusia, N. A. Cherepkov, A. Tancic, S. G. Shapiro, and L. Chernysheva, *Zh. Eksp. Teor. Phys.* **68**, 2023 (1975), [Sov. Phys. JETP **41**, 1012 (1975)].
- [25] M. Y. Amusia, N. A. Cherepkov, L. V. Chernysheva, D. M.

Davidović, and V. Radojević, *Phys. Rev. A* **25**, 219 (1982).

[26] W. R. Johnson and C. Guet, *Phys. Rev. A* **49**, 1041 (1994).

[27] Y. Cheng, L. Y. Tang, J. Mitroy, and M. S. Safronova, *Phys. Rev. A* **89**, 012701 (2014).

[28] M. Y. Amusia, N. A. Cherepkov, L. V. Chernysheva, and S. G. Shapiro, *J. Phys. B* **9**, L531 (1976).

[29] V. A. Dzuba, V. V. Flambaum, W. A. King, B. N. Miller, and O. P. Sushkov, *Phys. Scripta* **T46**, 248 (1993).

[30] G. F. Gribakin and J. Ludlow, *Phys. Rev. A* **70**, 032720 (2004).

[31] D. G. Green, *Phys. Rev. Lett.* **119**, 203403 (2017).

[32] D. G. Green, *Phys. Rev. Lett.* **119**, 203404 (2017).

[33] A. A. Abrikosov, L. P. Gorkov, and I. E. Dzyaloshinskii, *Methods of Quantum Field Theory in Statistical Physics* (Dover, New York, 1975).

[34]  $\mathfrak{Q}_E^\pm$  acts as  $\mathfrak{Q}_E^\pm \psi_\varepsilon(\mathbf{r}) = \int \Sigma_E^\pm(\mathbf{r}, \mathbf{r}') \psi_\varepsilon(\mathbf{r}') d\mathbf{r}'$ .

[35] See Ref. [27] for higher-order calculations.

[36] V. A. Dzuba and G. F. Gribakin, *Phys. Rev. A* **49**, 2483 (1994).

[37] There is a similarity between our approach and the combination of MBT with the configuration-interaction method for open-shell atoms [50].

[38] R. Brown, Q. Prigent, A. R. Swann, and G. F. Gribakin, *Phys. Rev. A* **95**, 032705 (2017).

[39] K. F. Canter, J. D. McNutt, and L. O. Roellig, *Phys. Rev. A* **12**, 375 (1975).

[40] K. Rytsola, J. Vettneranta, and P. Hautojarvi, *J. Phys. B* **17**, 3359 (1984).

[41] P. G. Coleman, S. Rayner, F. M. Jacobsen, M. Charlton, and R. N. West, *J. Phys. B* **27**, 981 (1994).

[42] M. Skalsey, J. J. Engbrecht, C. M. Nakamura, R. S. Vallery, and D. W. Gidley, *Phys. Rev. A* **67**, 022504 (2003).

[43] Y. Nagashima, T. Hyodo, K. Fujiwara, and A. Ichimura, in *The International Conference on the Physics of Electronic and Atomic Collisions, Vancouver, 1995, Abstracts of Contributed Papers* (1995).

[44] J. J. Engbrecht, M. J. Erickson, C. P. Johnson, A. J. Kolan, A. E. Legard, S. P. Lund, M. J. Nyflot, and J. D. Paulsen, *Phys. Rev. A* **77**, 012711 (2008).

[45] The FT+vdW data corresponds to the cut-off radius  $R_0 = 3.0$  a.u. in the model van der Waals potential [7].

[46] M. I. Barker and B. H. Bransden, *J. Phys. B* **2**, 730 (1969).

[47] D. G. Green and G. F. Gribakin, *Prog. Theor. Chem. and Phys.* (2018), [arXiv:1703.06980](https://arxiv.org/abs/1703.06980).

[48] Extrapolation in  $\ell_{\max}$  typically reduces the value of  ${}^1Z_{\text{eff}}$  by  $\sim 20\%$ , while extrapolation in  $n_{\max}$  is much less important, changing  ${}^1Z_{\text{eff}}$  by  $\lesssim 1\%$ .

[49] A. R. Swann, Ph.D. thesis, Queen's University Belfast (2017).

[50] V. A. Dzuba, V. V. Flambaum, and M. G. Kozlov, *Phys. Rev. A* **54**, 3948 (1996).